

4. THE MERCURY ENVIRONMENT

4.1 MERCURY THERMAL ENVIRONMENT

4.1.1 Planet Thermal Model

Because of the proximity to the Sun and the lack of any significant atmosphere, the surface temperature of Mercury largely depends on solar elevation and Mercury's orbital position. The temperature at the subsolar point, when Mercury is at perihelion, may be as high as 700 K, and the temperature over the night side drops to about 100 K.

For the purpose of this study, a simplified thermal model of the planet has been elaborated (Santovincenzo, 2000), under the following assumptions:

- no heat is generated inside the planet;
- no significant convective heat exchange takes place in the atmosphere of the planet;
- the surface is smooth (the model can take into account the presence of craters in specific areas, but this extension has not been implemented yet);
- only the conduction along the radial direction is considered in the thermal exchange; the heat transfer parallel to the surface is disregarded;
- no thermal radiation is considered;
- the inclination of the Mercury equator to the Sun equator is assumed = 0
- the planet internal structure consists of a crust and a core; only the heat transfer in the crust is estimated.

The surface of the planet is divided into 90 latitude x 36 longitude x 52 radial nodes. A total crust thickness of 5 m is analysed. The assumed thermal properties are given in Table 4.1-1 and Figure 4.1-1.

Property	Value
Albedo	0.07
Emissivity	0.9
Density (fine regolith-type)	1300 kg/m ³
Specific heat (regolith-type)	800 J/kgK
Conductivity (regolith-type)	Dependent on temperature and thickness (Figure 4.1-1)

Table 4.1-1: Planet thermal properties

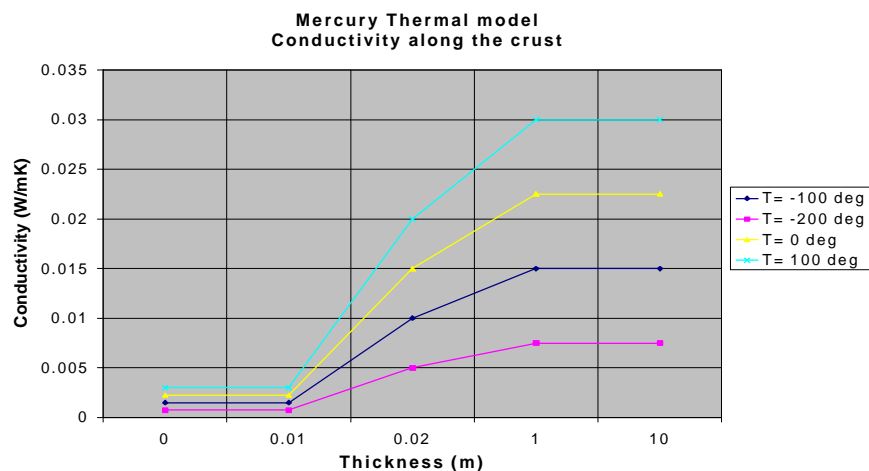


Figure 4.1-1: Mercury crust conductivity as a function of depth and temperature.

The crust properties derived from Moon soil are assumed to be applicable to Mercury.

A set of thermal balance equations and boundary conditions for the surface and internal nodes has been written and solved to derive the temperature field versus latitude, longitude, internal depth and time:

- for a node i on the illuminated side of the surface:

$$m_i c_i \frac{dT_i}{dt} = (1-a) \frac{Q_s}{d(t)^2} \cos I_i \cos \alpha_i(t) - \epsilon_i \sigma T_i^4 - K_{ik} (T_k - T_i),$$

- for a node i on the dark side:

$$m_i c_i \frac{dT_i}{dt} = -\epsilon_i \sigma T_i^4 - K_{ik} (T_k - T_i),$$

- for an internal node k :

$$m_k c_k \frac{dT_k}{dt} = K_{ki} (T_i - T_k) - K_{kj} (T_j - T_k),$$

- for the innermost boundary node:

$$T_j = const,$$

where:

$Q_s =$	solar constant at Earth (W/m^2),
$d =$	distance from the Sun (in AU),
$a =$	planet albedo,
$\epsilon =$	planet emissivity,
$\lambda_i =$	latitude of node i ,
$\alpha_i =$	angle between the Sun direction and the normal to the surface (function of longitude, rotation angle and revolution angles),
$K_{ij} =$	conduction exchange coefficient between node i and j .

The evolution of the temperature during half a Mercury day (one Mercury revolution) is shown in Figure 4.1-2. The same sequence is experienced simultaneously in the reverse order by the opposite side of the planet because of the 3:2 spin-orbit coupling.

Figures 4.1-3 to 4.1-5 show the surface temperature versus time at increasing latitudes for different longitudes. In all figures, the reference meridian (long = 0) coincides with the subsolar longitude when the planet is at the first perihelion of the Mercurian day.

The spin-orbit coupling and orbital eccentricity of Mercury also leads to the Sun elevation and surface thermal conditions remaining practically constant, for a relatively long period of time.

The low latitude regions in the vicinity of the reference meridian (5° in Figures 4-1.3 to 4-1.5) experience the largest temperature excursion. At higher longitudes (75°), less extreme values and variations are observed and the temperature is almost constant at longitudes around 115° for a significant duration between aphelion and perihelion. This effect arises because the variation of the solar elevation is balanced by the decrease of the distance from the Sun.

Peculiar regions on the surface of Mercury with stable temperatures for up to 80 Earth days can be found in the “late afternoon” and “early morning” when Mercury is at one of its perihelions. Figures 4.1-2 to 4-1.5 also show that the high latitude regions present the smallest variations in temperature and Earth-like values in the stable areas; they are, then, the most interesting locations for a possible landing. The effect of the terrain slope is also important; the temperatures can be significantly underestimated even for a slope of $15-20^\circ$ facing the Sun. This effect must not be ignored in local thermal analyses. These considerations have been taken into account for the calculation of optimal landing sites (Section 5.2.3).

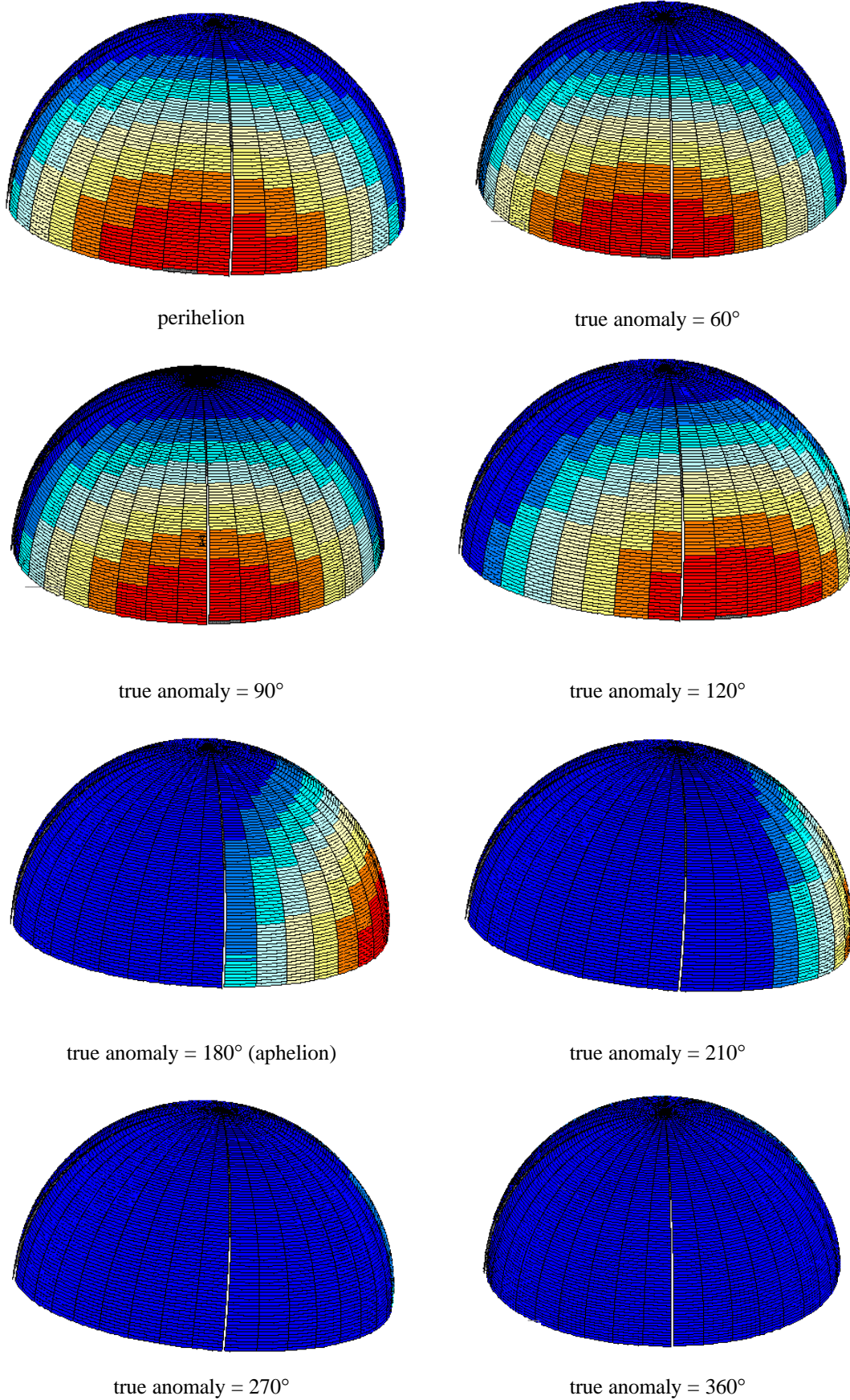


Figure 4.1-2: Mercury surface temperature distribution as a function of orbital position.

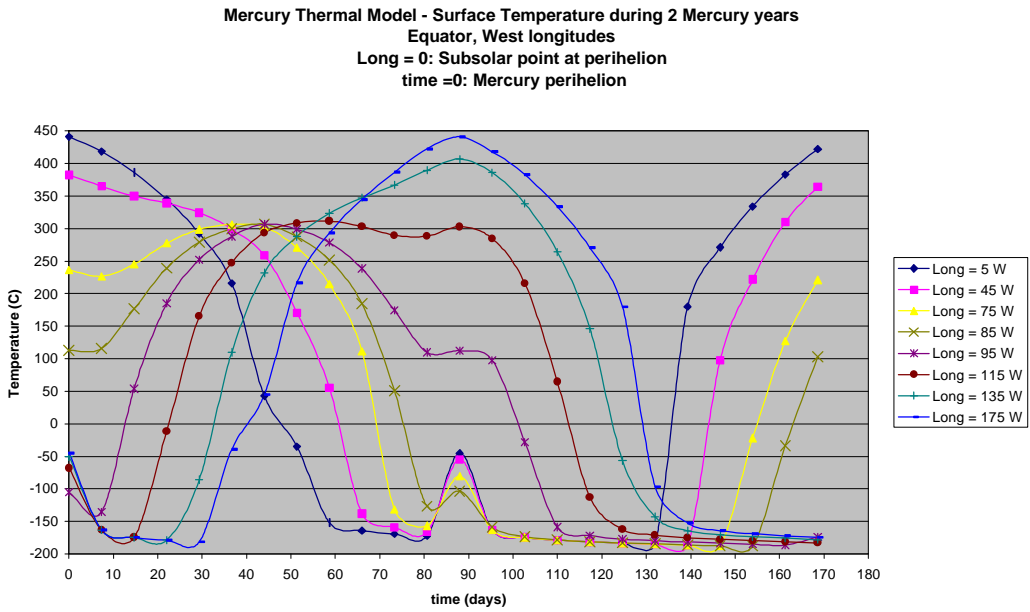


Figure 4.1-3: Variation of surface temperature in the equatorial regions (results are symmetrical for east and west longitudes).

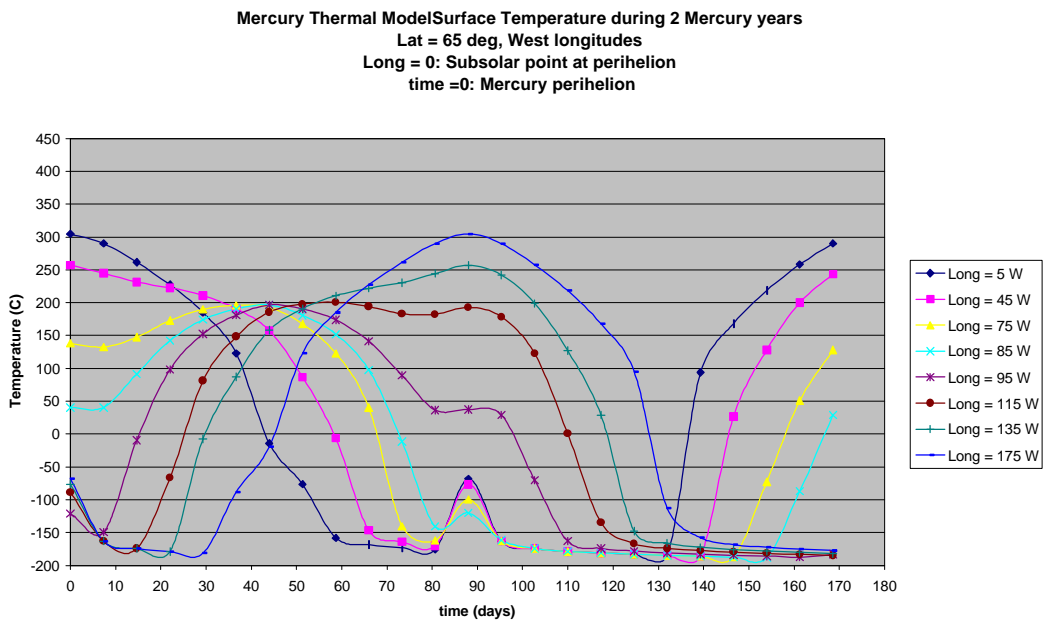


Figure 4.1-4: Variation of surface temperature at medium latitude.

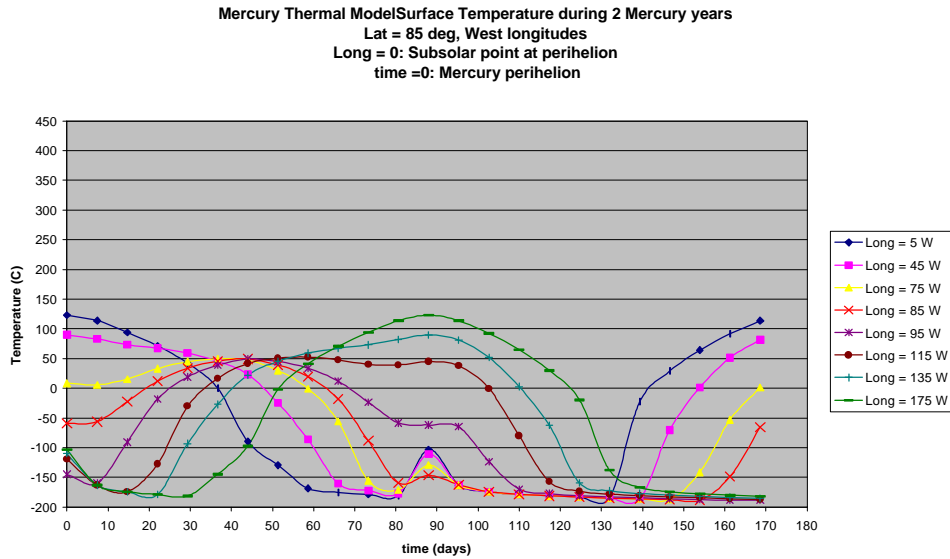


Figure 4.1-5: Variation of surface temperature at high latitude.

4.1.2 Spacecraft Thermal Modelling

The parameters influencing the thermal design of a spacecraft in orbit around Mercury are summarised in Table 4.1-2.

	Perihelion	Aphelion
Solar constant	14490 W/m ²	6290 W/m ²
Planetary flux at subsolar point, sunlit side	13614 W/m ²	7348 W/m ²
Equivalent temperature	700 K	600 K
Planetary flux at subsolar point, dark side	6 W/m ²	6 W/m ²
Equivalent temperature	100 K	100 K

Table 4.1-2: Planet thermal parameters

The surface temperature seen by a spacecraft varies significantly, both with spacecraft position and distance to the Sun (seasonal variation). Proper modelling of these variations is important for the calculation of the infra-red fluxes. Software packages that calculate IR fluxes (THERMICA or ESARAD) assume a planet at uniform temperature. The results must be corrected to account for the actual temperature distribution; a software routine was developed for this purpose, assuming $\alpha_{\text{planet}} = 0.89$ and $\epsilon_{\text{planet}} = 0.9$. The seasonal effect is taken into account by varying the subsolar temperature T_{ref} with distance from the Sun, as shown in Figure 4.1-6. The orientation of the orbital plane is taken in such a way that the pericentre is at the subsolar point when Mercury is at aphelion.

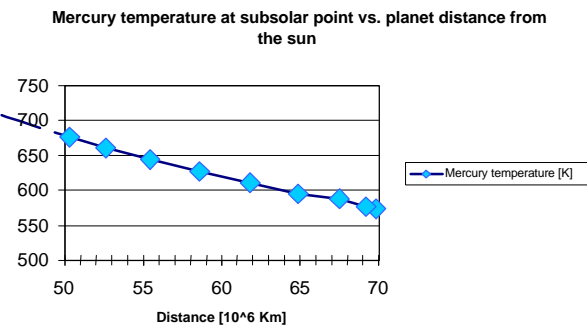


Figure 4.1-6: Temperature at subsolar point as a function of Sun distance.

4.2 PARTICLE RADIATION

4.2.1 Radiation Environment

The space radiation environment consists of magnetically trapped charged particles (around the planets with a significant magnetic field), solar energetic particles, and galactic cosmic rays (GCR). The penetrating particles pose the main problems to spacecraft, including upsets to electronics, payload interference, damage to electronics and deep dielectric charging.

For the Mercury mission, the main threat consists primarily of solar energetic particles. Solar protons are products of solar events, with energies in excess of several hundred MeV and peak fluxes in excess of 10^6 protons $\text{cm}^{-2} \text{s}^{-1}$ for protons with energies greater than 10 MeV. These events, though, are relatively rare, occurring primarily during periods of several years around solar maximum. The duration of individual events is usually of the order of days. The stochastic nature of these events requires an event based statistical treatment. As the expected fluence varies with heliocentric distance, the location of the spacecraft at the onset of a large event greatly influences the fluence encountered. To provide a total mission fluence, the time averaged heliocentric distance is used to scale the 1 AU model fluences. The operational phase fluence serves as a worst-case example. This is due to the assumption that a large event will occur when the spacecraft is close to the Sun, i.e. on orbit, instead of during the transfer phase. The large fluxes of energetic protons and heavier ions can contribute a large dose and increase upset rates in electronics and radiation induced background noise in detectors.

Figure 4.2-1 shows the predicted sun spot number at the epoch of the Mercury mission. It is apparent that, with the initial conditions assumed in this study (launch in the 2007 to 2010 time frame; two year cruise followed by 1 year presence at the planet) the Mercury orbit phase will occur at a time close to solar maximum.

At Mercury, the particle flux density is about 10 fold with respect to 1 AU. Figure 4.2-2 shows the proton fluence (Evans, 1999).

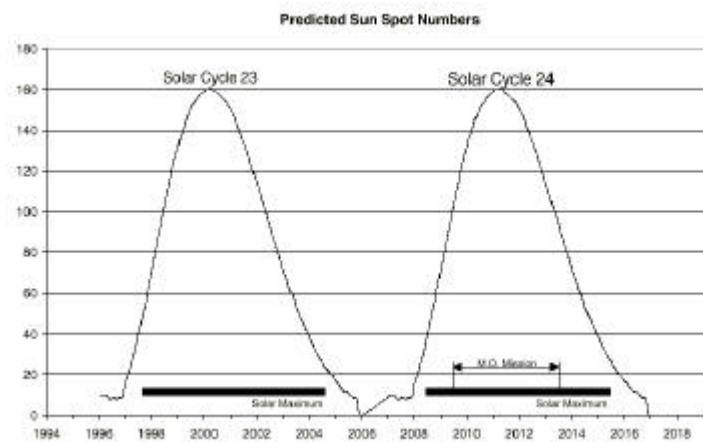


Figure 4.2-1: Sun spot number 1994-2020.

4.2.2 Radiation Effects and Measures for their Minimisation

The radiation effects on the spacecraft at Mercury include total dose, solar cell degradation and single event effects. The total dose effects on electronic parts and solar cell degradation is comparable to scientific missions in Earth orbit (e.g. the 10 year XMM mission), provided 4 mm Al equivalent shielding thickness is implemented (Figure 4.2-3).

Single Event Effects (SEE) due to protons pose problems in solar maximum periods.

Memories: SEE during solar proton events are about a factor of 10 higher than for missions at 1AU, therefore EDAC (error detection and correction) or other methods to reduce the SEU rate are necessary. It is expected that the SEE rate from galactic cosmic rays will be less than at 1 AU due to the attenuation of the GCR flux by the solar wind. The maximum SEU rate is about 10^{-10} SEU/(bit day);

for a comparison, the XMM requirement is 10^{-11} SEU/(bit day) for memories. Proton effects dominate in Mercury orbit and have to be evaluated in detail.

Linear parts: Linear parts on Mercury spacecraft suffer 10-fold the SEU effects of 1 AU missions. In periods of solar events, the SEU rate can reach up to 1000/day. Galactic Cosmic Ray (GCR) effects remain constant.

Proton induced SEU: The effects of protons on optocouplers are dramatic. Damage due to low energy protons (0.05 MeV) may be critical, but shielding by optics is sufficient to avoid this problem (no direct radiation exposure to payload system CCD). Effects of high-energy proton fluxes on CCD are unclear; research on CMOS sensor technology is in progress (at Daimler) for suitable space radiation applications.

Measures for minimising the radiation effects can be taken at system level (structures), at unit level (housing, electronics), and at part level (Keil 1999).

A reduction of solar proton induced effects can be expected if structure materials have a low yield for secondary effects, e. g. neutrons. Materials with high carbon content, e. g. CFRP, C/SiC, B₄C etc., are recommended. The current design assumption is a CFRP structure with low Z material. At unit level, housing must be made from high and low Z materials (second layer shielding), while electronics must use SEU-safe designs. At parts level, spotshielding is to be used, if necessary, to minimise mass, in combination with radhard, i.e. single event robust parts (SOI and SOS technology).

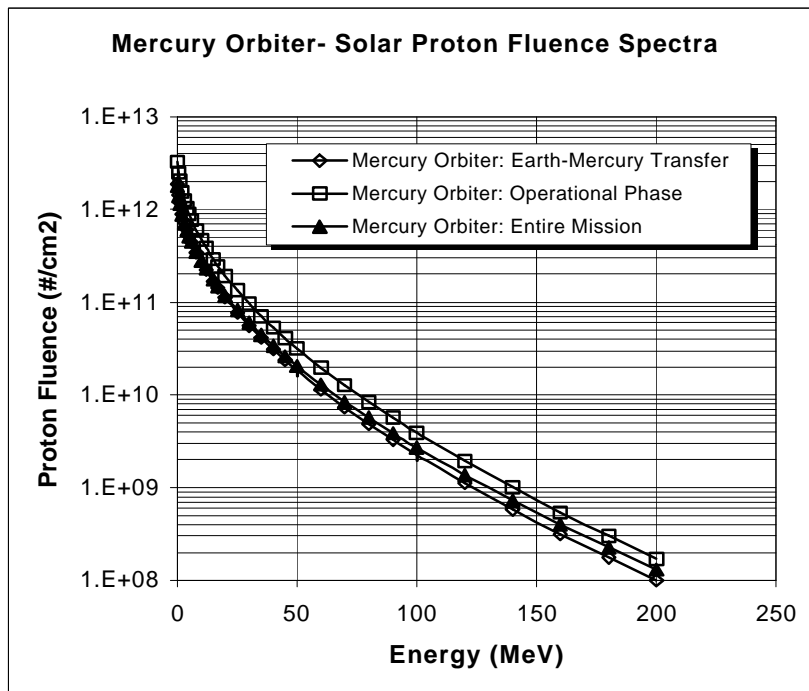


Figure 4.2-2: Mercury mission proton fluence.

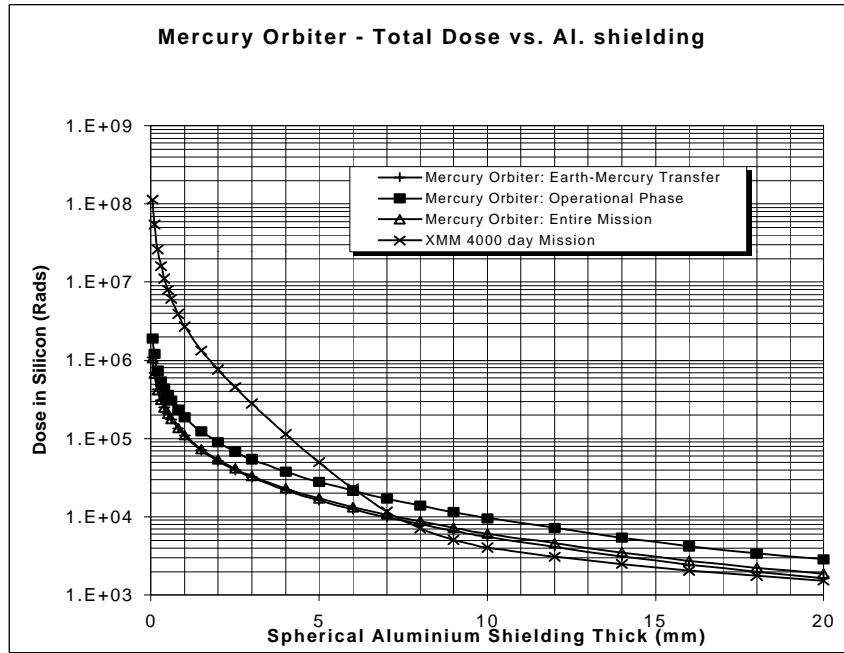


Figure 4.2-3: Total dose comparison Mercury vs. XMM.